

# Accurate Compact MOSFET Modeling Scheme for Harmonic Distortion Analysis

B. Iñiguez<sup>\*</sup>, R. Picos<sup>\*\*</sup>, I. Kwon<sup>\*\*\*</sup>, M. S. Shur<sup>\*\*\*\*</sup>, T. A. Fjeldly<sup>\*\*\*\*\*</sup>, and K. Lee<sup>\*\*\*</sup>

**Abstract**—We discuss and develop a compact MOSFET modeling scheme in order to obtain accurate descriptions of the drain current and its derivatives up to the 5<sup>th</sup> order. We have analyzed the physical effects which govern the behaviour of the 3<sup>rd</sup> derivative in long and deep-submicron channel MOSFETs. Our modeling agrees well with experimental data and describes continuous transitions between operating regimes, thanks to the use of continuous functions, which do not introduce any artificial peaks.

## I. INTRODUCTION

An adequate MOSFET model for distortion analysis should not only provide accurate current-voltage characteristics, but should also exhibit good agreement with higher order derivatives of the drain current, which determine the main contributions to higher-order harmonics [1-3]. Most MOSFET models do not satisfactorily describe distortion. One of the reasons is that the modeling equations of some physical effects, such as mobility, series resistance, and velocity saturation, are not sufficiently accurate for describing the derivatives. Another reason is that the interpolation

functions, used to provide smooth transitions between regimes, often induce artificial peaks and kinks when the modeled characteristics are differentiated.

A surface potential-based charge sheet model [4-7], can provide accurate expressions of harmonics up to the third order. However, in order to ease circuit design, it would be desirable to develop a model which could, at the same time, keep the physical basis of surface potential-based models and use simpler expressions which may allow direct parameter extraction techniques for most of the model parameters.

An alternative to surface potential-based models are the charge linearization models, which result from a linearization of the inversion charge density with respect to the surface potential [8-16]. This approach leads to simpler expressions of the drain current, total charges, and the small-signal parameters, and allows for easy incorporation of short-channel effects needed to model scaled-down devices, and for the development of direct techniques to extract most of the parameters [9]. Besides, the effect of the device parameters on the harmonic performance is easier to estimate.

In this paper, we present a compact model, based on charge linearization, which provides acceptable accuracy up to the 5<sup>th</sup> derivative of the drain current. This model follows the approach used by previous charge linearization models, such as UCCM [11-14] and EKV v2.6 [9], but its accuracy for the  $n^{\text{th}}$  derivatives is increased thanks to the use of an appropriate mobility model (accounting for the main scattering mechanisms), a proper incorporation of short-channel effects (velocity saturation, channel-length modulation, DIBL, and series resistance), and the utilization of more adequate interpolation functions. The physical basis of the model

---

Manuscript received May 31, 2004; revised September 15, 2004.

<sup>\*</sup> DEEEA, Universitat Rovira i Virgili, Avda. Països Catalans 26, 43007 Tarragona Spain. E-mail: binyigue@etse.urv.es

<sup>\*\*</sup> Department of Physics, Universitat de les Illes Balears, Cra. De Valldemossa, Km. 755, 07071 Palma de Mallorca, Spain

<sup>\*\*\*</sup> Department of Electrical Engineering and Computer Science, KAIST, Taejon, 305-701 Korea

<sup>\*\*\*\*</sup> ECSE Department Rensselaer Polytechnic Institute, 110 8th Street, Troy, 12180NY, USA

<sup>\*\*\*\*\*</sup> UniK- University Graduate Center, 70 Postboks, Kjeller, N-2027. Norway

allows for easy determination of the influence of each physical effect on the higher-order derivatives of the channel current, in particular on the 3<sup>rd</sup> derivatives. It is shown that some effects, such as velocity saturation and channel length modulation, make the shape of the 3<sup>rd</sup> derivative of a deep-submicron MOSFET very different from that for a long-channel device. We also demonstrate the problems of other conventional modeling techniques to accurately fit the experimental 3<sup>rd</sup> derivatives. In particular, it is shown that artificial peaks are often found. In contrast, our model provides reasonably good agreement with experimental results through all operating regimes for MOS transistors with effective channel lengths down to 0.11  $\mu\text{m}$ .

## II. MODEL

Our compact charge linearization model is based on the unified charge control model (UCCM). This model is derived from a charge-sheet model by linearizing the channel charge density in terms of the surface potential:

$$a(n_c - n_0) + \eta V_{th} \ln\left(\frac{n_c}{n_0}\right) = V_{GS} - V_T - \alpha V_{CS} \quad (1)$$

where  $\eta$  is the subthreshold ideality factor,  $V_{th}$  is the thermal voltage,  $V_T$  is the threshold voltage,  $n_c$  is the local (inversion) carrier density,  $V_{CS}$  is the channel voltage (referred to the source),  $\alpha$  is the body effect parameter,  $n_0 = \frac{\eta V_{th} C_{ox}}{2q}$  and  $a = \frac{q}{C_{ox}}$ ,  $C_{ox}$  being the oxide capacitance per unit area. This charge control model reduces to the one used in EKV v2.6 model if  $V_T$  and  $\alpha$  have the values resulting from the linearization of the inversion charge density at the substrate [17].

Equation (1) has no analytical solution for the inversion charge density. However, several approximate explicit expressions for the inversion charge density in terms of the voltage bias have been proposed. One of the most commonly used expressions is:

$$n_c = 2n_0 \log\left[1 + 0.5 \exp\left(\frac{V_{GS} - V_T - \alpha V_{CS}}{\eta V_{th}}\right)\right] \quad (2)$$

However, these expressions ignore the increase of the

surface potential with the gate voltage in strong inversion, which may affect the accuracy of the high order derivatives of the channel current. On the other hand, the effect of non-pinned surface potential in strong inversion is inherent to UCCM. Equation (1) can be solved for  $n_c$  in terms of the Lambert's W function:

$$n_c = 2n_0 \text{LambertW}\left(\frac{1}{2} \exp\left(\frac{1}{2} + \frac{V_{GS} - V_T}{\eta V_{th}}\right)\right) \quad (3)$$

Our channel current model is derived using the Gradual Channel Approximation, which is valid in the non-saturated part of the channel. In channel potential formulation, it can be written as:

$$I_{ds} = \mu W q n_c \frac{dV_{CS}}{dx} \quad (4)$$

In surface potential formulation, the drain current can be written as:

$$I_{ds} = W q \left[ -\mu V_{th} \frac{dn_c}{dx} + n_c v \right] \quad (5)$$

where  $v$  is the drift velocity.

The first term in (5) is the contribution due to diffusion and the second term is the contribution due to drift.

The drift velocity depends on the lateral field (field in the direction of the channel). At low lateral fields, it is proportional to the field; at high lateral fields it saturates to a value ( $v_{sat}$ ). An appropriate and simple velocity-field relationship is the one proposed by Sodini, which is quite accurate for nMOSFETs.

$$v = \begin{cases} \frac{\mu_n E_x}{1 + \frac{\mu_n E_x}{2v_{sat}}} & E_x \leq \frac{2v_{sat}}{\mu_n} \\ v_{sat} & E_x \geq \frac{2v_{sat}}{\mu_n} \end{cases} \quad (6)$$

where  $\mu_n$  is the carrier mobility that depends on the normal fields, and  $E_x$  is the absolute value of the lateral field. It can be written as  $E_x = \frac{d\psi_s}{dx}$ , where  $\psi_s$  is the surface potential.

Since velocity saturation is relevant only in strong inversion, where the drift term dominates, we can write, in the non-saturated portion of the channel:

$$I_{ds} = Wqn_c \frac{\mu_n d\psi_s / dx}{1 + \frac{\mu_n d\psi_s / dx}{2v_{sat}}} \frac{dV_{CS}}{dx} \quad (7)$$

(It is also possible to incorporate the mobility dependence on the electron density in the channel (or on the normal component of the electric field, see [14], Section 6.8.2 and expressions given below.) The channel current is obtained by integration using UCCM. In order to obtain an analytical solution, we consider an effective mobility,  $\mu_{eff}$ , independent of  $x$ .

The channel current is finally written in terms of the channel charge densities at the source and drain ends:

$$I_{ds} = \frac{W}{\alpha L_{eff}} \frac{\mu_{eff} q}{1 + \delta_0 \frac{\mu_{eff} (n_s - n_d)}{\alpha L_{eff} v_{sat}}} \left[ \eta v_T (n_s - n_d) - a \frac{n_s^2 - n_d^2}{2} \right] \quad (8)$$

where  $L_{eff}$  is the effective channel length (including its reduction by channel length modulation).  $\delta_0$  is a factor introduced in order to assure continuity of the derivatives at  $V_{DS}=0$ .

The channel charge density at the source is obtained from UCCM using  $V_{CS}=0$ . In order to calculate the inversion charge density at the drain, we cannot use the long-channel UCCM equation (1) in the saturation regime, where GCA cannot be applied in the saturated portion of the channel (near the drain). However, UCCM can be extended using the saturation voltage ( $V_{CS}=V_{dsat}$ ) instead of  $V_{CS}=V_{DS}$ , which depends on the relationship used between velocity and lateral field. In order to make the model continuous, a suitable smoothing expression of the effective drain-source voltage,  $V_{dseff}$ , is needed, which tends to  $V_{DS}$  in the triode regime and to  $V_{dsat}$  in the saturation regime.

$$a(n_d - n_0) + \eta V_{th} \ln\left(\frac{n_d}{n_0}\right) = V_{GS} - V_T - \alpha V_{dseff} \quad (9)$$

The accuracy of the high-order derivatives is critically dependent on the choice of this interpolation function. Some of the expressions of  $V_{dseff}$  proposed in the literature are:

$$V_{dseff} = V_{dsat} - V_{dsat} \frac{\log[1 + \exp(A_{TS}(1 - V_{ds}/V_{dsat}))]}{\log[1 + \exp(A_{TS})]} \quad (10)$$

(see [18,19])

$$V_{dseff} = \frac{V_{ds}}{[1 + (V_{ds}/V_{dsat})^m]^{1/m}} \quad (11)$$

(see [15])

$$V_{dseff} = V_{dsat} - \frac{1}{2} \left[ V_{dsat} - V_{ds} - \delta + \sqrt{(V_{dsat} - V_{ds} - \delta)^2 + 4\delta V_{dsat}} \right] \quad (12)$$

where  $A_{TS}$ ,  $m$  and  $\delta$  are fitting parameters (see [20])

The expression for the saturation voltage consistent with the Sodini velocity-field relationship is [13,14]:

$$V_{dsat} = \frac{2an_s V_L}{an_s + 2V_L} \quad (13)$$

$$\text{where } V_L = \frac{\mu_{eff} L}{v_{sat}} \quad (14)$$

This expression, (13), tends to the saturation voltage in strong inversion, but not in weak inversion, where the saturation voltage (caused by diffusion) is approximately  $2V_{th}$ . In order to calculate the channel charge density at the drain using the UCCM equation (1), we can use an interpolation function which tends to  $2V_{th}$  in weak inversion, and to  $V_{dsat}$  in strong inversion [21] However, this interpolation function may introduce artificial peaks in the high order derivatives.

We found that the following expression for the channel charge density at the drain [16], which depends on the one calculated at the source and the expression of  $V_{dsat}$  given by (13), is very adequate for high order derivatives:

$$n_d = n_s - \alpha a V_{dseff} \left( 1 + 2 \frac{\exp(-V_{ds}/V_{th})}{1 + \exp\left(a \frac{n_s}{V_{th}}\right)} \right) \quad (18)$$

The accuracy of the higher order derivatives is critically dependent on the effective mobility model. The mobility decreases with increasing normal electric field due to the increase of phonon and surface roughness scattering. Some of the proposed expressions of the effective mobility, in terms of the effective normal field are:

$$\mu_{eff} = \frac{\mu_0}{1 + \theta E_n} \quad (19)$$

(see, for example [6])

$$\mu_{eff} = \mu_0 (1 - \theta_\mu E_n) \quad (20)$$

(see [14,16,17]). Here  $\mu_0$ ,  $\theta$  and  $\theta_\mu$  are fitting parameters.

The normal field can be written in terms of the inversion and depletion charge densities as [13,14]:

$$E_n = \frac{qn_c/2 - q_b}{\epsilon_{si}} \quad (21)$$

where  $q_b$  is the depletion charge density (per unit area), which is calculated as  $q_b = \gamma C_{ox} \sqrt{\phi_B + V_{CB}}$ , where  $\gamma$  accounts for the body effect,  $V_{CB}$  is the channel voltage referred to the bulk, and  $\phi_B$  is the semiconductor bulk potential.

A more accurate expression, which accounts separately for phonon and surface roughness scattering is [17]:

$$\mu_{eff} = \frac{\mu_0}{1 + \theta_{ph} E_n^{1/3} + \theta_{sr} E_n^2} \quad (22)$$

In many models, the normal field used in the effective mobility expression, is calculated at the source end. However, this may be not accurate enough to model the higher order derivatives at high  $V_{DS}$ . We will use an average normal field in the effective channel, defined as:

$$E_n = \frac{q(n_s + n_d)/2 - (q_{b,s} + q_{b,d})}{2\epsilon_{si}} \quad (23)$$

The series resistance can be included in the expression of the effective mobility up to first order as [16,19]:

$$\mu_{effR} = \frac{\mu_{eff}}{1 + a_R} \quad (24)$$

where  $\mu_{eff}$  is the expression of the effective mobility without the series resistance and

$a_R = \mu_{eff} C_{ox} R_T \frac{W}{L} (an_d + \alpha V_{dseff}/2)$ ,  $R_T$  being the total series resistance.

This expression of the effective mobility is used in the equation for the saturation voltage, with  $V_{dseff} = V_{dsat}$ , and  $n_d$  calculated at this voltage. There is no explicit solution for the saturation voltage. However, a first-order estimation, such as the long channel saturation voltage  $V_{dsat} = (V_{gs} - V_T)/\alpha$ , can be used in the expression of the effective mobility.

The reduction of effective channel length due to channel length modulation is obtained from a quasi-two dimensional analysis as [16]:

$$L_{sat} = l_a \log \left( \frac{C_a + \sqrt{C_a^2 + K_a^2}}{K_a} \right) \quad (25)$$

where  $C_a = V_{ds} - V_{dseff}$  and  $K_a = 2l_a v_{sat} / \mu_{eff}$ ,  $l_a$  being the characteristic length.

The threshold voltage expression includes the DIBL effect [6]:

$$V_T = V_{T0} - \sigma V_{ds} \quad (26)$$

where  $V_{T0}$  is the drain-bias independent threshold voltage and  $\sigma$  is the DIBL parameter (increasing with decreasing channel length).

The source-drain symmetry, with the resulting continuity at  $V_{DS}=0$ , is guaranteed by using an appropriate expression for  $\delta_0$  ( $\delta_0 = \delta_L V_{dseff}/V_{dsat}$ ) [17] ( $\delta_L$  being a constant), and an equation of the threshold voltage resulting from the linearization of the inversion charge density at the substrate; in this case, the bulk bias parameter,  $\alpha$ , does not depend on the source-bulk voltage.

### III. RESULTS

We have compared our modeling with measurements obtained from a 0.18  $\mu\text{m}$  KAIST process. Most of the parameters were extracted using direct techniques, in the regimes where they are relevant. This is mainly possible because our modeling is based on charge linearization. The threshold voltage was extracted as the gate voltage, which maximizes  $d^2 I_d / V_{GS}^2$ , that is, the voltage that makes  $d^3 I_d / V_{GS}^3 = 0$ . The direct techniques used to extract most of the parameters are explained in [13,14].

In order to clearly identify the different mechanisms affecting the 3<sup>rd</sup> derivative, we first study the 3<sup>rd</sup> derivative of a long-channel device (Fig. 1-3). It is equivalent to study the nonlinearities of the device. Series resistance effect, velocity saturation and channel length modulation are negligible for these long-channel devices. According to the long-channel theory,  $d^3 I_d / V_{GS}^3 = 0$  in both the linear and saturation regimes. We observe in the figures that the magnitude of the 3<sup>rd</sup> derivative has a value close to zero, except in subthreshold, at the transition from below to above threshold, and at the transition from saturation to the linear regime. There is a peak value when the source end goes from weak to strong inversion and a second peak when, in long-channel devices, it is the drain end which goes from weak to strong inversion (Fig. 2). At  $V_{GS} = V_T$ ,  $d^3 I_d / V_{GS}^3 = 0$ , what means that this corresponds, in

dB, to the dip between the two peaks at low  $V_{DS}$  (Fig. 1 and 3).

We proved that some models cannot reproduce the peak found between the saturation and the linear regimes at moderate and high drain voltages. This is critically dependent on the expression of  $V_{dseff}$ . The expression (11) does not get that peak when normal values of  $m$  are used. Only using abnormally high values of  $m$  it is possible to observe the peak; however these high values of  $m$  originate artificial peaks or dips for the 3<sup>rd</sup> derivative (Fig. 1) at low  $V_{DS}$ . The expression (10) reproduces quite accurately the peak at the transition between saturation and linear regime for high  $V_{DS}$ ; however, it also produce artificial peaks or dips for the 3<sup>rd</sup> derivative (Fig. 1) at low  $V_{DS}$ .

We demonstrate in Fig. 1-3 that using the third expression of  $V_{dseff}$ , we accurately reproduce all peaks for the 3<sup>rd</sup> derivative, for high and low  $V_{DS}$ , without any artificial peaks, dips nor glitches.

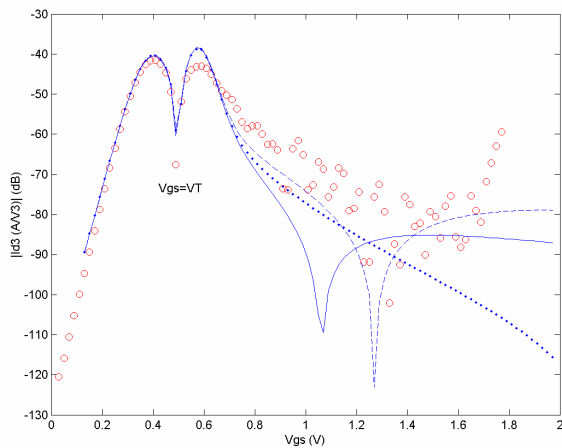


**Fig. 1.** Measured (symbols) and modeled  $d^3 I_d / V_{GS}^3$  (in dB) characteristics at  $V_{DS} = 0.1$  V for a transistor with  $L = 5$   $\mu\text{m}$ . Model with mobility given by (19) (solid line), (20) (dotted line) and (22) (dashed line).  $V_{dseff}$  calculated according to (12)

We have also compared the effect of the different mobility models in Fig. 3. The mobility model affects the width of the peaks. The most conventional mobility model (19) is not accurate enough for the 3<sup>rd</sup> derivative. The model of Eq (20) [11] works well for the 3<sup>rd</sup> derivative at high  $V_{DS}$  (especially at moderate  $V_{GS}$ ), but is far less accurate at low  $V_{DS}$  and higher  $V_{GS}$  (the values of zero-3<sup>rd</sup> derivative are significantly lower than those observed experimentally). The more complete mobility

model of Eq (22) produces much better results. We note that in order to fit the width of the 1<sup>st</sup> peak at high  $V_{DS}$  (Fig. 2) it is necessary to take into account the effect of the drain voltage on the effective normal field used in the effective mobility expression (23). Many models just use, in the effective mobility expression, the normal field at the source end, therefore ignoring the drain voltage dependence; as a result, the resulting accuracy of the 3<sup>rd</sup> derivative at high  $V_{ds}$  is lower.

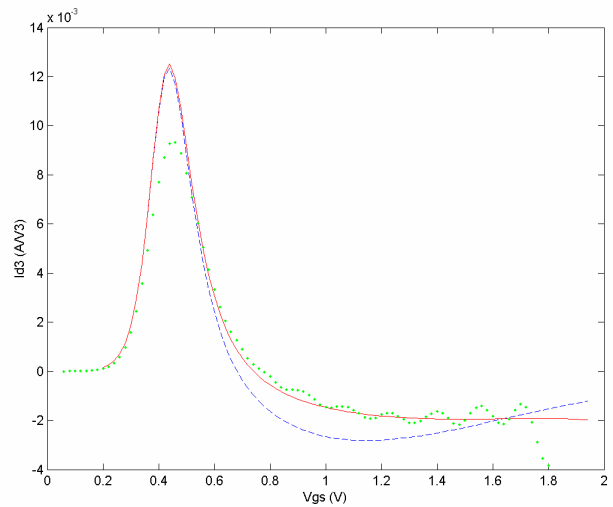


**Fig. 2.** Measured (dotted line) and modeled (lines)  $d^3 I_d / V_{GS}^3$  characteristics at  $V_{DS} = 1.8$  V for a transistor with  $L = 5$   $\mu\text{m}$ . We have used (12) and (22).  $E_n$  calculated at the source end (dashed line) or as an average value using (23) (solid line).

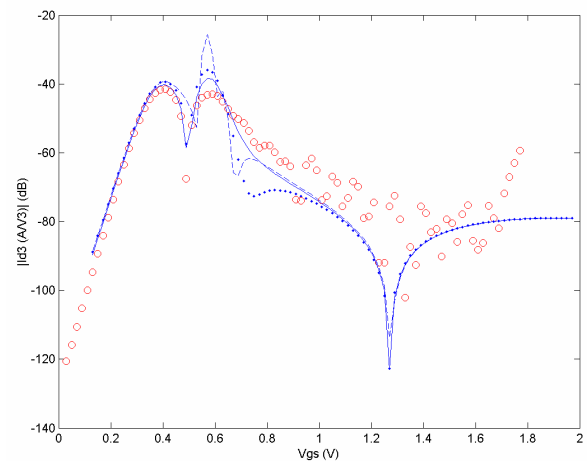


**Fig. 3.** Measured (symbols) and modeled  $d^3 I_d / V_{GS}^3$  characteristics (in dB) at  $V_{DS} = 0.1$  V for a transistor with  $L = 5$   $\mu\text{m}$ . Mobility given by (22).  $V_{dseff}$  calculated according to (10) with  $A_{TS} = 12$  (dotted line), (11) with  $m = 4.5$  (dashed line) and (12) with  $\delta = 0.01$  (solid line).

On the other hand, the fitting with the experimental 5<sup>th</sup>

derivative, using the mobility model of (21) and the expression of  $V_{dseff}$  of (12), is quite acceptable (Fig. 4), since the position of peaks are reasonably well predicted.

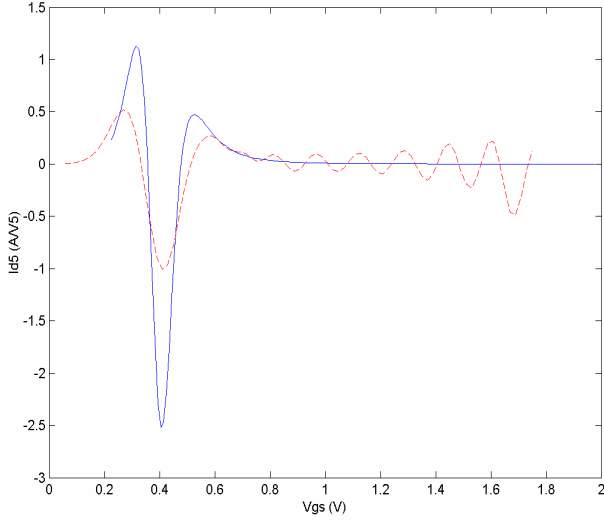


**Fig. 4.** Measured (dashed line) and modeled (solid line)  $d^3 I_d / V_{GS}^3$  characteristics at  $V_{DS}=1.8$  V for a transistor with  $L=5$   $\mu\text{m}$ . We have used (12) and (22).

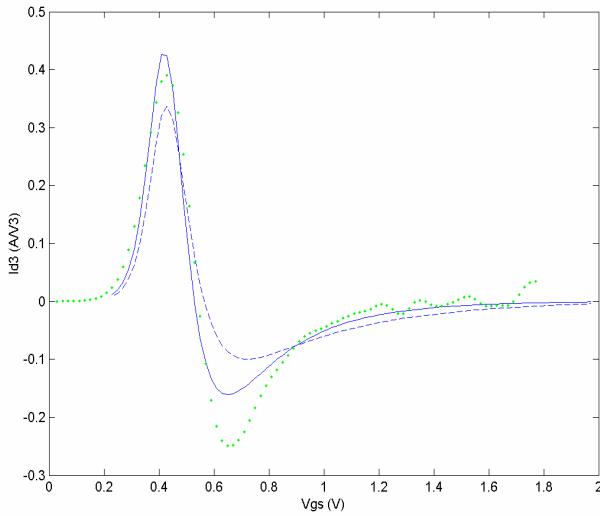


**Fig. 5.** Measured (dotted line) and modeled  $d^3 I_d / V_{GS}^3$  characteristics at  $V_{DS}=1.8$  V for a transistor with  $L=0.18$   $\mu\text{m}$ . Solid line: complete model. Dashed line: model without series resistance and channel length modulation.

The shape of the 3<sup>rd</sup> derivative is quite different for submicron and deep-submicron devices, as we note in Fig. 5-10, especially at high  $V_{DS}$ . This has to be due to short-channel effects. We did not observe anymore the negative peak at the transition between the saturation and the linear regimes; we found that it is masked by the

velocity saturation effect. But we observed a new negative peak (in linear scale) in the moderate inversion region, near threshold (Fig. 5). We demonstrated that this peak is caused by channel length modulation and the series resistance effect. The DIBL effect was also found to be significant and has an influence on the 3<sup>rd</sup> derivative in subthreshold and near threshold. Our complete model, using the suitable mobility and  $V_{dseff}$  models, and taking into account short-channel effects, fits reasonably well the experimental values of the 3<sup>rd</sup> derivative at low and high  $V_{DS}$ . The fitting of the 3<sup>rd</sup> derivative of the output characteristics (with respect to  $V_{DS}$ ) is also acceptable (Fig. 8-9). Besides, we obtained a reasonable description of the 5<sup>th</sup> derivative (Fig 10).

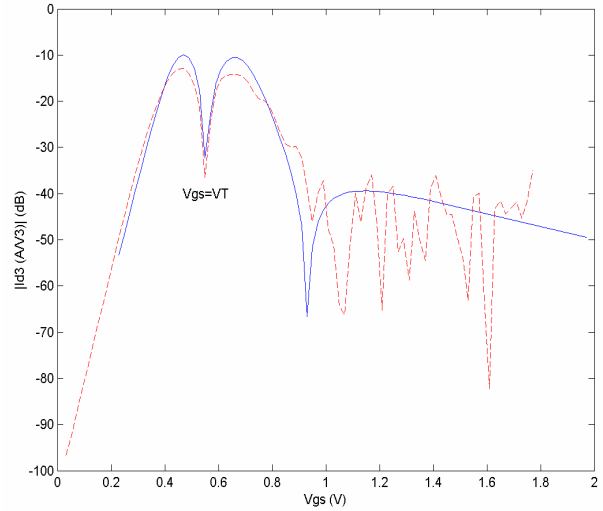


**Fig. 6.** Measured (dashed line) and modeled (solid line)  $d^3 I_d / V_{GS}^3$  (in dB) characteristics at  $V_{DS}=0.1$  V for a transistor with  $L=0.18$   $\mu\text{m}$ .

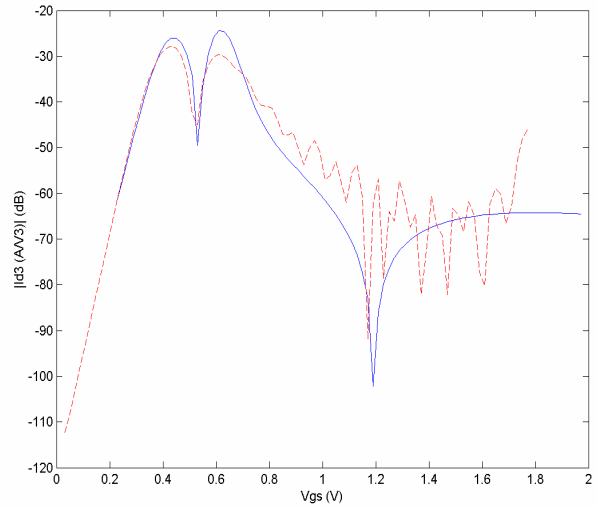


**Fig. 7.** Measured (dashed line) and modeled (solid line)  $d^3 I_d / V_{GS}^3$  characteristics at  $V_{DS}=0.1$  V for a transistor with  $L=1.0$   $\mu\text{m}$ .

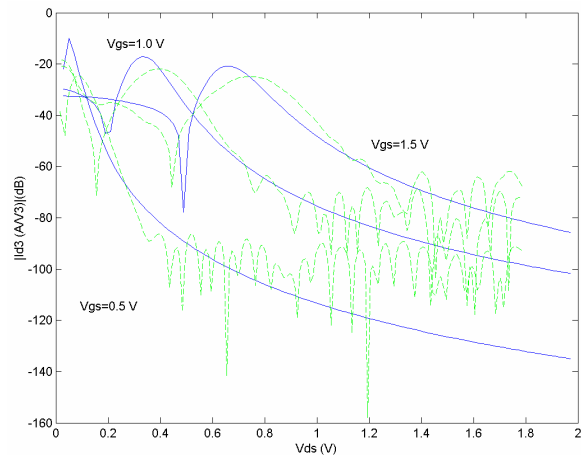


**Fig. 8.** Measured (dashed lines) and modeled (solid lines)  $d^3 I_d / V_{DS}^3$  (in dB) versus  $V_{DS}$  characteristics at  $V_{GS}=0.5, 1.0, 1.5$  V for a transistor with  $L=1.0$   $\mu\text{m}$ .

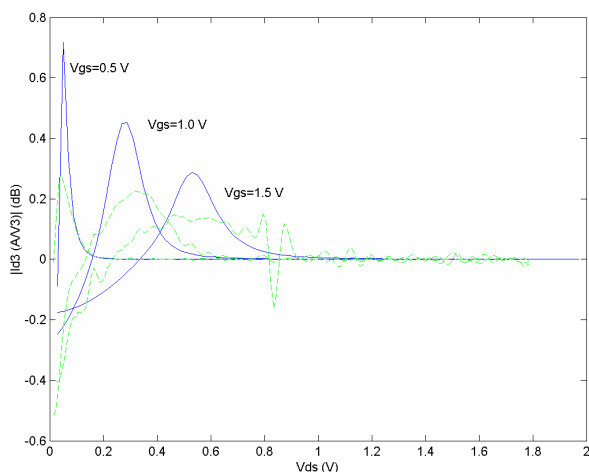


**Fig. 9.** Measured (dashed lines) and modeled (solid lines)  $d^3 I_d / V_{DS}^3$  characteristics at  $V_{GS}=0.5, 1.0, 1.5$  V for a transistor with  $L=0.35$   $\mu\text{m}$ .

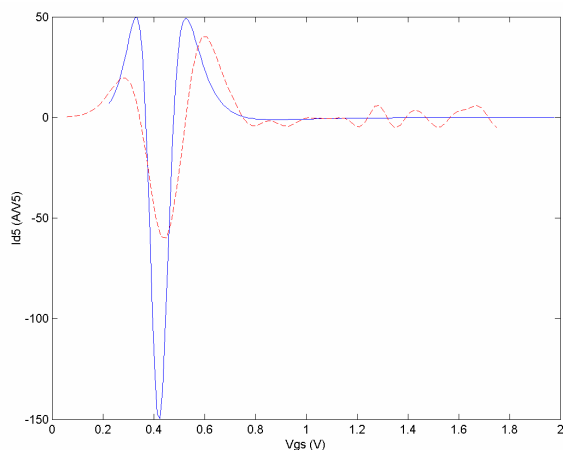


**Fig. 10.** Measured (dashed line) and modeled (solid line)  $d^5 I_d / V_{GS}^5$  characteristics at  $V_{DS}=1.8$  V for a transistor with  $L=0.18$   $\mu\text{m}$ .

### IV. CONCLUSION

We have presented a compact MOSFET modeling scheme, which provides accurate descriptions of the channel current and its derivatives up to the 5<sup>th</sup> order through all operating regimes. The modeling is based on an appropriate analysis of the physical effects which determine the behaviour of the high order derivatives, and on the use of adequate smoothing functions which do not introduce any artificial peaks nor glitches in the high order derivative characteristics.

### ACKNOWLEDGEMENT

This work was supported by MICROS Research Center, an Engineering Research Center under Korea Science and Engineering Foundation.

### REFERENCES

- [ 1 ] K. Lee , “The Impact of nm CMOS Technology of Wireless Circuit and System,” *Proc of the 2003 Asia-pacific Workshop on Fundamentals and Applications of Advanced Semiconductor Devices*
- [ 2 ] Shin, Hyungcheol ; Minkyu Je ; Jeonghu Han ; Kwyro Lee, *Microelectronics Reliability*, vol. 43 no. pp.601-609, Apr. 2003
- [ 3 ] R. Van Langevelde and F. M. Klaassen, *IEEE Trans. on Electron Devices*, vol. 44, no. 11, pp. 2044-2052, November 1997.
- [ 4 ] R. van Langevelde, et al., *Electron Devices Meeting, 2000. IEDM Technical Digest. International* , Pages:807 – 810, 10-13 Dec. 2000
- [ 5 ] R. van Langevelde and F. M. Klaassen, *Solid-State Electronics*, vol. 44, no., pp. 409-418, March 2000.
- [ 6 ] Y. P. Tsividis, *Operation and Modeling of the MOS Transistor*, 2<sup>nd</sup> ed., New York: McGraw Hill, 1999.
- [ 7 ] T. -L. Chen and G. Gildenblat, *Solid-State Electronics*,

- vol. 45, pp. 335-339, 2001.
- [ 8 ] K. Joardar, et al., *IEEE Trans. on Electron Devices*, vol. 45, pp. 134-148, January 1998.
- [ 9 ] J. –M. Sallese, et al., *Solid-State Electronics*, vol. 47, pp. 677-683, 2003.
- [10] A.I.A.Cunha, M.C.Schneider, C.Galup-Montoro, “An MOS Transistor Model for Analog Circuit Design”, *IEEE Journ. Solid-State Circuits*, Vol. 33, N° 10, pp.1510-1519, October 1998.
- [11] C. –K. Park, et al., “A unified current-voltage model for long-channel nMOSFETs,” *IEEE Trans. on Electron Devices*, vol. 38, pp. 399-406, February 1991.
- [12] M. S. Shur, T. A. Fjeldly, T. Ytterdal and K. Lee, “Unified MOSFET model,” *Solid-State Electronics*, vol. 35, no. 12, pp. 1795-1802, December 1992.
- [13] K. Lee, M. Shur, T. A. Fjeldly and T. Ytterdal, *Semiconductor Device Modeling for VLSI*, Prentice-Hall, 1993.
- [14] T. A. Fjeldly, T. Ytterdal and M. Shur, *Introduction to Device Modeling and Circuit Simulation*, New York, John Wiley & Sons, 1998.
- [15] B. Iñiguez and E. García-Moreno, *IEEE Transactions on Computer-Aided Design of Integrated Circuits and Systems*, vol. 14, no. 2, pp. 163-166, February 1995 .
- [16] B. Iñiguez and E. García-Moreno , *Analog Integrated Circuits and Signal Processing* (Kluwer), vol. 13, no. 3, pp. 241-259, July 1997.
- [17] S. B. Chiah, et al., *IEEE Electron Device Letters*, vol. 25, no. 5, May 2004
- [18] C. C. McAndrew, B. K. Bhattacharyya and O. Wing, *IEEE Electron Device Letters*, vol. 12, pp. 565-567, October 1991.
- [19] N. D. Arora, et al., *IEEE Trans. on Electron Devices*, vol. 41, pp. 988-997, June 1994.
- [20] Y. Cheng, et al., *IEEE Trans. on Electron Devices*, vol. 44, pp. 277-287, February 1997.
- [21] J. A. Power and W. A. Lane, *IEEE Trans on Computer-Aided Design*, vol. 11, pp. 1418-1425, November 1992

The authors' biography's and photo's are not available at the time of publication.